Originally published as:

Hydrothermal spinel, corundum and diaspore in lower oceanic crustal troctolites from the Hess Deep Rift

Toshio Nozaka[1]*, Romain Meyer[2,4], Robert P. Wintsch[3], and Bryan Wathen[3]

[1] Department of Earth Sciences, Okayama University, 3-1-1 Tsushima-naka, Okayama 700-8530, Japan

[2] Centre for Geobiology and Department of Earth Science, University of Bergen, Allegaten 41, NO-5006 Bergen, Norway

[3] Department of Geological Sciences, Indiana University, 1005 E. 10th Street, Bloomington, IN 47405, USA

[4] Present Address: GFZ German Research Centre for Geosciences, Telegrafenberg, D-14473 Potsdam, Germany

*Corresponding author.   Telephone: +81-86-251-7883.   Fax: +81-86-251-7895.
E-mail: nozaka@cc.okayama-u.ac.jp

Abstract

Aluminous spinel, corundum and diaspore are reported from intensely altered parts of primitive troctolites recovered from IODP Site U1415 at the Hess Deep Rift. The spinel is green-colored, has an irregular shape, has low Cr concentrations, and so distinct from primary igneous chromite. Corundum and diaspore occur mainly at the rims of green spinel grains with a texture suggesting a sequential replacement of spinel by corundum, and then corundum by diaspore. The green spinel is associated with anorthite and pargasite, which is overgrown by tremolite that forms coronitic aggregates with chlorite around olivine. These petrographic observations are supported by pressure-temperature pseudosections, which predict spinel + pargasite stability field, and tremolite/hornblende + chlorite field at lower temperature conditions. From these pseudosections and simplified system phase diagrams, estimated formation temperature conditions calculated at 2 kbar are 650-750 °C for spinel + pargasite, 410-690 °C for tremolite/hornblende + chlorite, 400-710 °C for corundum, and < 400 °C for diaspore. Because the aluminous spinel occurs in the domains that were previously occupied by magmatic plagioclase, and because spinel-bearing rocks characteristically have high Al_2O_3/CaO and Al_2O_3/SiO_2 ratios, it is likely that the stabilization of spinel was caused by the loss of Ca^{2+} and $SiO_2(aq)$ in high-temperature hydrothermal fluids. The results of this study suggest that (1) the concentrations of aluminous phases in the lower oceanic crust are presently underestimated, and (2) chemical modification of the lower oceanic crust due to high-temperature hydrothermal metasomatic reactions could be common near spreading axes.

Introduction

The oceanic crust is the largest boundary zone between Earth's lithosphere and hydrosphere, and seawater-rock interaction in the oceanic crust has an important role in Earth's dynamics, in particular global geochemical cycling. Hydrothermal alteration of igneous rocks is one of the most conspicuous products of the water-rock interaction. Despite growing evidence from rocks tectonically exposed at the seafloor (e.g., Hékinian et al. 1993; Dick et al. 2008; Lissenberg et al. 2013; Sauter et al. 2013; Rouméjon et al. 2015), the lack of samples collected *in situ* from the lower oceanic crust has hindered progress in understanding geochemical cycling. For example, questions remain about how deeply water can penetrate into the plutonic oceanic crust and how hydrothermal alteration proceeds in these lower oceanic crustal lithologies.

To fill this gap of knowledge, Expedition 345 of the Integrated Ocean Drilling Program (IODP) was designed to drill and recover the deepest-level oceanic crustal rocks formed at the East Pacific Rise (EPR) with the principal objectives to understand crustal accretion and hydrothermal processes at fast-spreading ridges. We studied the recovered rocks at sea and have documented some basic characteristics (Gillis et al. 2014a, b). Here we report more specific results from onshore petrological studies on the hydrothermal alteration of these rocks. One key discovery is the occurrence of hydrothermal green spinel, corundum and diaspore. Although green spinel and corundum have been reported from ophiolitic metagabbros and pyroxenites and their origin and tectonic implications have been discussed (e.g., Kornprobst et al. 1990; Morishita and Arai 2001; Abily et al. 2011), this study is the first to report these aluminous phases from *in-situ* oceanic crust. We first focus on their modes of occurrence and chemical compositions, and then discuss the physico-chemical conditions for their formation.

Geological setting

At the Hess Deep Rift young plutonic crust formed at the fast-spreading EPR has been exposed by the

westward propagation of the Cocos-Nazca spreading axis (Fig. 1; Lonsdale 1988; Francheteau et al. 1990; Wiggins et al. 1996; Gillis et al. 2014b). The Ocean Drilling Project (ODP) Leg 147 took advantage of this tectonic window by drilling the exposures at the Hess Deep Rift. At ODP Sites 894 and 895 (Fig. 1), respectively, gabbroic rocks from the upper parts of the lower crustal section and peridotites from the upper mantle section were recovered (e.g., Mével et al. 1993). Zircons in gabbroic samples collected from the Hess Deep intra-rift ridge yielded U-Pb ages from 1.27 to 1.42 Ma (Rioux et al. 2012).

The IODP Expedition 345 drilled Site U1415 between 4675 and 4850 m water depths along the southern slope of the intra-rift ridge at Hess Deep. The main target of this expedition was the lower gabbro section of intact, fresh oceanic lithosphere between the upper gabbro section drilled at ODP Site 894 and the upper mantle section at Site 895. Of 16 holes at Site U1415, the two deepest holes, U1415J and U1415P reached a depth of ~110 m below seafloor. The dominant lithologies are relatively primitive olivine gabbro and troctolite with Mg# [molar $100MgO/(MgO+FeO)$] between 76 and 89, with more than half of them showing distinct modal and grain size layering (Gillis et al. 2014a, b). A variety of alteration minerals were also found in assemblages suggesting temperature conditions from amphibolite to zeolite facies (Gillis et al. 2014b).

Material and methods

A few grains of pale green spinel in altered troctolites were identified during shipboard microscopic observations. As these grains seemed to be restricted to intervals containing significant amounts of amphibole and chlorite showing coronitic texture, we intensively sampled cores with abundant coronas (Fig. 2) in addition to relatively fresh parts for comparison. Polished thin sections were prepared for microscopic observations and chemical analyses of minerals using an electron probe microanalyzer, JEOL JXA-8230 at Okayama University. Quantitative microprobe analyses were carried out with an accelerating voltage of 15 kV and a beam current of 20 nA. Standards used were natural or synthetic oxides and silicates. The applied matrix corrections followed the procedures of Bence and Albee (1968), using alpha factors of Nakamura and Kushiro (1970). The identification of corundum and diaspore was confirmed by supplementing optical characteristics and chemical compositions with Raman shift spectra, using a Raman spectrometer, JASCO NRS-3100 at Okayama University, with 488 nm laser excitation, a

100x microscope objective lens, and a diffraction grating with 1800 grooves/mm.

Thin section billets were analyzed for major elements by X-ray fluorescence (XRF) spectrometry with a Phillips PW1404 at the University of Bergen, using fused glass discs (0.96 g ignited sample powder with 6.72 g Spectromelt A-10 flux. Available geochemical rock data obtained with the shipboard inductively coupled plasma–atomic emission spectrometry (ICP-AES; Gillis et al. 2014b) were used for comparison.

Pressure-temperature (P-T) pseudosections in the system Na_2O-CaO-FeO-MgO-Al_2O_3-SiO_2-H_2O and phase diagrams in the system CaO-MgO-Al_2O_3-SiO_2-H_2O were constructed using the software Perple_X ver. 6.6.8 (Connolly 2005, 2009; updated 2013) with the dataset of Holland and Powell (1998, updated 2002) and the CORK equation of state of fluids (Holland and Powell 1991, 1998). Adopted solution models were Diener et al., (2007) for clinoamphibole, Holland and Powell (1998) for olivine and spinel, Holland and Powell (1996) for orthopyroxene and clinopyroxene, Holland et al. (1998) for chlorite, and Holland and Powell (2003) for plagioclase.

Aqueous activity diagrams in the system CaO-MgO-Al_2O_3-SiO_2-H_2O were constructed using the software SUPCRT (Johnson et al. 1992) as modified following the computation methods of Zimmer et al. (2016) with thermodynamic properties of minerals (Holland and Powell 2011), aqueous species (Shock et al. 1989) and aqueous silica (Stefánsson 2001).

Results

Modes of occurrence of spinel, corundum and diaspore

Green spinel occurs exclusively in centimeter- to decimeter-scale intensely altered zones of troctolites (Fig. 2), indicating its hydrothermal origin. Roughly estimated modal compositions in thin sections of these intensely altered rocks are 40-50 % amphibole, 40-50 % chlorite, < 2 % green spinel, < 1 % corundum + diaspore, < 2 % relic olivine + mesh-textured or pseudomorphic serpentine/clay + opaque minerals, < 5 % relic plagioclase + pseudomorphic clinozoisite/prehnite, < 2 % relic clinopyroxene, and < 2 % relic chromite + pseudomorphic magnetite. The distribution of minerals within a thin section is heterogeneous, and intensely altered samples commonly consist of amphibole-rich and chlorite-rich

3

domains. Green spinel commonly occurs as irregularly shaped, discrete grains in the chlorite-rich domains (Fig. 3a-h). The amphibole-rich and chlorite-rich domains are interpreted as formerly occupied by igneous olivine and plagioclase, respectively, based on the comparison of the size, shape and distribution of olivine and plagioclase in fresh troctolites. This interpretation is supported by the general observations of altered troctolites with a coronitic texture, where olivine is partially or completely replaced by a pseudomorphic aggregate of amphibole and plagioclase by a chlorite aggregate (Nozaka and Fryer 2011; Gillis et al. 2014b). The coronitic amphibole + chlorite, with an almost equal or slightly higher amount of chlorite, occur in many altered troctolites from Hess Deep irrespective of the presence of spinel. Amphibole varies in chemical composition from pargasite, through hornblende to tremolite reflecting the nearby existence of spinel as mentioned later, but is commonly colorless or pale green in accordance with its magnesium-rich compositions. Hence, it is impossible to distinguish the different species of amphibole under the optical microscope.

Corundum and diaspore occur as replacements of green spinel. At an early stage of the replacement, corundum and diaspore mainly occur at the rims of green spinel grains; as the amount of diaspore and corundum increases, spinel relics become smaller and have increasingly irregular shapes (Fig. 3b-g). In general, typical diaspore occurs in elongated-platy or acicular forms (Deer et al. 1992). In the Hess Deep samples, however, diaspore has an equant or short prismatic shape similar to that of corundum. Furthermore, corundum is commonly accompanied by diaspore, and the grain size of diaspore increases in accordance with that of corundum (compare Fig. 3e and g; more evident with crossed-polars though not shown). These textures suggest the replacement of spinel by corundum, and then the pseudomorphic replacement of corundum by diaspore. Tiny inclusions (< 1 μm in diameter) of iron sulfide are sporadically distributed within diaspore.

Macroscopic (millimeters wide) or microscopic (< 40 μm wide) amphibole veins within plagioclase, which are common in the upper gabbro section at Hess Deep (Manning and MacLeod 1996; Manning et al. 1996) are lacking. Instead chlorite microveins within plagioclase are common in the samples examined in this study. The chlorite microveins are connected to chlorite that encloses plagioclase. Some of the enclosing chlorite form coronitic aggregates with tremolite, whereas others form complex layers with serpentine that replaces adjacent olivine. Compared with these samples, the chlorite microveins within plagioclase are less abundant in spinel-bearing samples, and thus seem to be

4

independent of spinel formation. Serpentine, clay and opaque minerals (mainly magnetite and Fe-sulfides) replacing olivine are later-stage alteration minerals. Clinozoisite and prehnite locally occur replacing plagioclase, but shows no direct relationship to the occurrence of spinel and coronitic amphibole, suggesting that they are later-stage alteration minerals as well.

Compositional variations of minerals

Representative microprobe analyses are given in Table 1, and the complete dataset is provided as Electronic Supplementary Material. Relics of primary magmatic plagioclase with anorthite (An) contents of 81-89 mol%, and olivine with forsterite (Fo) contents of 82-88 mol% are common in relatively fresh troctolitic samples. Primary spinel (chromite) contains $Cr_2O_3 > 40$ wt% (Table 1).

Green spinel has a compositional range from spinel (*sensu stricto*) to pleonaste (Fig. 4) with X_{Mg} [molar Mg/(Mg+ total Fe)] ranging mostly from 0.7 to 0.8 and with a significant deficiency in Cr in contrast to primary chromite. Corundum and diaspore have ~98 wt% and ~80 wt% of Al_2O_3, respectively. In the proximity of corundum (and its diaspore pseudomorph), each spinel grain becomes richer in Fe (Fig. 3b, c), and chlorite is slightly enriched in Al and Fe (Fig. 3b-g). Such a compositional zoning implies that corundum and nearby chlorite formed at a physico-chemical condition different from those for spinel and surrounding chlorite.

Amphibole is variable in composition from pargasite through hornblende to tremolite (Fig. 5). Pargasite (Si < 6.5 pfu, X_{Mg} = 0.83-0.87 in most samples) occurs exclusively in green spinel-bearing samples and mainly in proximity of the green spinel crystals (Figs. 3h, 5). In many samples examined, regardless of whether or not they contain spinel, tremolite and subordinate amounts of hornblende occur as coronitic or pseudomorphic aggregates replacing olivine or as overgrowths of clinopyroxene. The Si content of the coronitic amphiboles in most Hess Deep samples varies from 6.6 to 7.9 pfu, and X_{Mg} from 0.90 to 0.97. In spinel-bearing samples, individual pseudomorphic aggregates of tremolite after olivine are rimmed by zones of pargasite or hornblende, and these pargasite/hornblende crystals are overgrown by tremolite (Fig. 3h-j). This textural relationship clearly suggests that tremolite formation postdates pargasite and hornblende formation. Tremolite is poorer in Fe than pargasite, and a small amount of magnetite is commonly associated with tremolite but not with pargasite.

5

In the proximity of green spinel, primary plagioclase is replaced by secondary plagioclase, which is almost pure anorthite (An = 98-99 mol%) and contains tiny (< 30 μm long) crystals of pargasite (Fig. 3k-m). Chlorite, which encloses spinel, cuts both the primary and secondary plagioclase (Fig. 3k-m), suggesting its formation at a later stage.

The relationships of the observed assemblages and chemical compositions of minerals are summarized in a traditional ACF diagram (Fig. 6). The general parallel course of the tie lines indicates a close approach to equilibrium between amphibole and chlorite solid solutions, although the equilibrium is perturbed probably by the effect of later alteration. The chemical compositions of minerals systematically vary in harmony with mineral association. The most aluminous chlorite and amphibole (pargasite) compositions are found in spinel-bearing rocks.

Rock compositions and P-T pseudosections

Of the four metamorphic spinel-bearing samples analyzed (Table 2), one (U1415J-18R-1_67-69 cm) is an unusual rock within the drilled rock succession, with a low Mg# (~70) and abundant modal magnetite, whereas the remaining three samples (U1415J-18R-1_8-14, 59-62, and 62-65 cm) are similar to typical Expedition 345 troctolites in their high Mg# (84-88) but significantly different in that the three samples have normative corundum (Table 2). The peraluminous geochemical character of the spinel-bearing rocks is noticeable when compared with the shipboard data from Holes J and P (Gillis et al. 2014b). The MgO and Al_2O_3 contents of all the rocks (Fig. 7a) are roughly consistent with the proposed general MORB-system cumulate crystallization trend in Gillis et al. (2014a). However, the spinel-bearing rocks have distinguishably higher Al_2O_3/CaO mole ratios, showing a contrast to shipboard samples, most of which have Al_2O_3/CaO ratios lower than 1.0 and lack normative corundum (Fig. 7b). Although one spinel-bearing sample (U1415J-18R-1_67-69 cm; Table 2) has a slightly lower Al_2O_3/CaO ratio (< 1.0), a shipboard sample reporting the highest Al_2O_3/CaO ratio and normative corundum (Fig. 7b) was obtained in immediate proximity to U1415J-18R-1_67-69 cm, and therefore the rocks in this interval should have, despite the small-scale heterogeneity, on average a peraluminous composition. When compared with relatively fresh troctolites analyzed in this study, the spinel-bearing rocks also have higher Al_2O_3/SiO_2 ratios (Fig. 7b). In general, Na_2O contents also affect the amount of normative corundum, but they are

very low (< 0.5 wt%) in the primitive troctolites from Hess Deep and no systematic variation related to normative and modal mineralogy was detected.

Pressure-temperature pseudosections were constructed for the whole-rock compositions given in Table 2, in order to estimate temperature conditions for the formation of spinel + pargasite + plagioclase because of the lack of appropriate thermometry for plagioclase with An > 90 mol%. We assumed the saturation of H_2O because the spinel-bearing rocks are intensely altered with only small amounts of relic magmatic minerals. These pseudosections successfully predict spinel-bearing and spinel-free mineral assemblages (Fig. 8), thus supporting our petrographic observations. In addition, the validity of the pseudosections is supported by predicted modal proportions and chemical compositions of secondary minerals, which show a consistency with observations; i.e., spinel (~3 vol%, X_{Mg} ~0.75) and pargasite (1-16 vol%, ~6.3 Si pfu) occur in the high-temperature spinel-pargasite field, and tremolite/hornblende (16-34 vol%) and chlorite (50-56 vol%) are abundant at lower temperatures.

Discussion

Conditions of spinel formation

Temperature conditions

It is evident from textures, mineral chemistry, and pseudosection calculations, that spinel + pargasite ± anorthite is the earliest-stage and highest-temperature alteration assemblage observed in the lower plutonic crustal section at Hess Deep. Although Al-rich chlorite could coexist with this assemblage (Fig. 6), this coexistence is not clear from textural observations and not supported by P-T pseudosections. The ranges of P-T conditions predicted by pseudosection modeling for amphibole-bearing assemblages among the six samples analyzed are compared in Fig. 9. The stability field of pargasite + spinel overlaps in all four spinel-bearing samples at approximately 700 °C. Because these samples were collected from the same section 1.5 m long (U1414J-18R-1), their alteration conditions should be almost the same, and the overlapping P-T range is the most likely condition for the spinel + pargasite assemblage. A minimum pressure of ~1.4 kbar for this assemblage is predicted from the overlapping P-T range. A maximum

pressure is provided from seismic data that reported a crustal thickness of 5-7 km with a water depth of ~3 km at the EPR spreading axis near the Galapagos microplate (Zonenshain et al. 1980). Although the inferred pressure conditions have uncertainty because of the complex geologic structure of the Hess Deep Rift (e.g., Francheteau et al., 1990), the steep slope of reaction curves in the P-T diagram provides temperature conditions of 650-750 °C for spinel + pargasite formation (Fig. 9).

These temperature conditions for spinel + pargasite are overlapping with highest-temperature estimates using amphibole-plagioclase geothermometry for the alteration including macroscopic or microscopic amphibole veins in the Hess Deep upper gabbro section, ~720-750 °C (e.g., Manning et al., 1996; Kirchner and Gillis, 2012). Coogan et al. (2002) have pointed out the similarity of temperatures for amphibole formation between upper and lower gabbro sections, and discussed its implications on seawater permeability and cooling of oceanic lower crust at different distances from the ridge axis. The formation of spinel is also localized but is associated with centimeter- to decimeter-scale alteration zones, much wider than the amphibole veins reported. It is unrealistic that such a considerable degree of high-temperature alteration took place at a distal off-axial region without thermal metamorphism of gabbroic host containing lower-temperature alteration minerals. Therefore, the spinel + pargasite assemblage is interpreted as a product of near-axis hydrothermal activity. The similar temperature conditions throughout upper to lower gabbro sections could reflect a thermal structure with steep isotherms near the spreading axis (Maclennan et al. 2004).
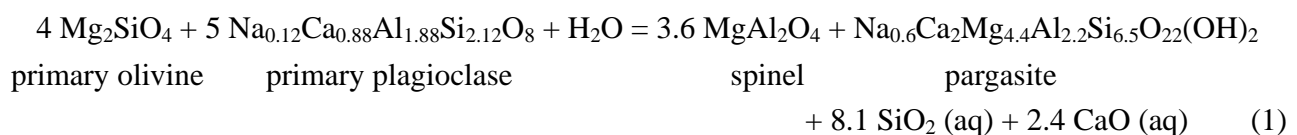
Chemical conditions

The transformation of magmatic olivine and plagioclase to metamorphic assemblages in troctolites are indicated by switching tie lines in Fig. 6, but the explanation for the observed composition-paragenesis relationships is not straightforward. Because the assemblage of spinel + pargasite + secondary anorthite requires an aluminous system composition (Fig. 6), it appears to be reasonable to expect that the assemblage occurs in plagioclase-rich (richer than the intersection of plagioclase-olivine and spinel-amphibole tie lines) troctolites rather than olivine-rich troctolites. However, the contents of Al_2O_3 of rocks analyzed in this study (Table 2) appear to be insufficient for the formation of the aluminous assemblage (Fig. 6). It is evident that the spinel formation does not require large amounts of plagioclase
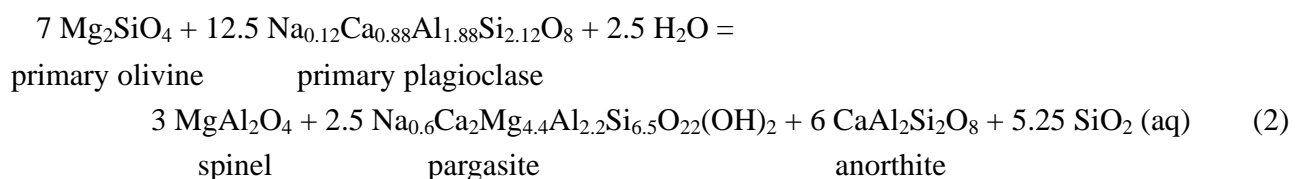
8

in original troctolites but just requires the presence of reactive plagioclase as the source of Al. In fact, spinel occurs in chlorite-rich (i.e., Al-rich) domains after plagioclase, where chlorite could form at a later stage, rather than in the amphibole-rich domains after olivine (Fig. 3h, i). It is clear that the crystallization of spinel from plagioclase requires the local loss of Ca and Si and the local gain of Mg, whereas olivine requires counteracting loss and gain of these elements to form amphibole.

In addition to the microscopic intergranular transfer of elements, a larger-scale metasomatic chemical modification is suggested by the fact that spinel-bearing rocks have normative corundum (Table2, Fig. 7b), which is uncommon in mafic magmatic systems. This chemical modification is the most plausible cause of the enlargement of the spinel and cordierite stability fields (Fig. 8a), which are generally unexpected in anhydrous plutonic rocks of troctolitic compositions. Aluminum solubility in H_2O is quite low (e.g., Dolejš and Manning, 2010), and the immobility of Al during high-temperature hydrothermal alteration of the Hess Deep troctolites is supported by the facts that spinel and chlorite are restricted to the proximity of plagioclase. The high Al_2O_3/CaO ratios of spinel-bearing rocks, therefore, suggest that dissolution and removal of CaO and the resulting increase in much less soluble Al_2O_3 is essential for spinel formation. In addition, removal of SiO_2 could also have taken place because the spinel-bearing rocks have higher Al_2O_3/SiO_2 ratios than spinel-free troctolites analyzed in this study (Fig. 7b). In contrast, removal or addition of MgO is not detected and no effect of MgO variation on spinel formation is indicated (Fig. 7a).

The spinel grains occur in association with pargasite and secondary anorthite. The specific reaction leading to the production of spinel is elusive; however, using representative microprobe data (Table 1) and assuming the simplified system Na_2O-CaO-MgO-Al_2O_3-SiO_2-H_2O and the mobility of CaO and SiO_2 discussed above, a mass-balanced reaction can be written:

$$4\ Mg_2SiO_4 + 5\ Na_{0.12}Ca_{0.88}Al_{1.88}Si_{2.12}O_8 + H_2O = 3.6\ MgAl_2O_4 + Na_{0.6}Ca_2Mg_{4.4}Al_{2.2}Si_{6.5}O_{22}(OH)_2$$

primary olivine   primary plagioclase   spinel   pargasite

$$+\ 8.1\ SiO_2\ (aq) + 2.4\ CaO\ (aq) \qquad (1)$$

or

$$7\ Mg_2SiO_4 + 12.5\ Na_{0.12}Ca_{0.88}Al_{1.88}Si_{2.12}O_8 + 2.5\ H_2O =$$

primary olivine   primary plagioclase

$$3\ MgAl_2O_4 + 2.5\ Na_{0.6}Ca_2Mg_{4.4}Al_{2.2}Si_{6.5}O_{22}(OH)_2 + 6\ CaAl_2Si_2O_8 + 5.25\ SiO_2\ (aq) \qquad (2)$$

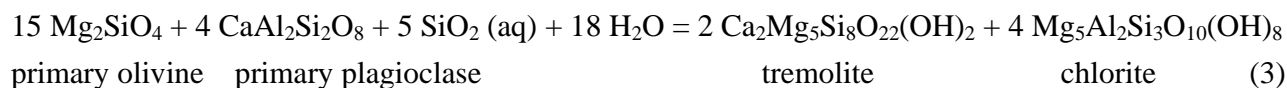spinel   pargasite   anorthite

Calculations using thermodynamic properties for minerals (Holland and Powell 1998) indicate a total solid products/reactants volume proportion of ~0.6 and ~0.9 for Reaction 1 and 2, respectively. The extreme volume loss up to 0.6 seems unrealistic, and therefore the amount of CaO released in Reaction 1 is probably a maximum estimate.

Although previous studies on the alteration of oceanic crust have shown that Ca may not always be removed under lower amphibolite-facies conditions up to 550 °C (e.g., Ferry 1985; Seyfried 1987), our results suggest that Ca-loss can take place at higher temperatures. Because the increase and decrease of CaO activity during alteration of oceanic crust are generally associated with the variations of Mg concentration and pH of aqueous fluids (e.g., Seyfried 1987), the compositions of the aqueous fluids attending the formation of spinel are examined in terms of activities of Ca^{2+}, Mg^{2+} and H^+ with variable SiO_2 activity. Higher acidity and/or lower SiO_2 activity is required for spinel stability than for tremolite + chlorite corona formation (Fig. 10), showing a contrast to much lower acidity during low-temperature alteration of seafloor basalts and peridotites (e.g., Seyfried 1987; Bach et al. 2004; Bach and Klein 2009).

Conditions of amphibole-chlorite corona formation

The tremolite + chlorite aggregates forming corona or pseudomorphs after olivine that reacted with plagioclase are more widely observed than spinel + pargasite in the primitive gabbroic rocks recovered from Site U1415. These coronitic minerals have magnesian compositions (X_{Mg} = 0.90 to 0.97). Such highly magnesian coronas are also abundant in primitive gabbroic rocks recovered from the Atlantis Massif at the Mid-Atlantic Ridge and interpreted as a product of amphibolite-facies alteration (Nozaka and Fryer 2011). Amphibolite-facies conditions for the corona formation in the primitive troctolites from Hess Deep are also indicated by coronitic amphibole compositions (Si = 6.8-7.9 pfu) and by the absence of assemblage of albite and zoisite (or clinozoisite) with the coronas (Fig. 8). The rimming relationships described above suggest that tremolite formed at a later stage than pargasite, and there is no evidence for deformation suggestive of an intense tectonic activity during the formation of the different types of amphibole (Fig. 3h-j). Therefore it is most likely that the tremolite + chlorite coronas formed during the cooling of lower crust at a depth similar to that of the spinel + pargasite formation. The P-T pseudosections predict temperatures between 410 and 690 °C for the corona formation (Fig. 9).

The reaction that produces the coronitic assemblage is described by the crossing tie lines of Fig. 6. Using idealized formulae and balanced on Al, Ca and Mg, a possible corona-forming reaction is written (Nozaka and Fryer 2011):
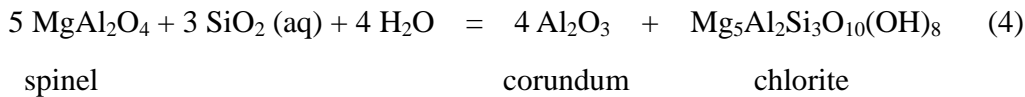
$$15\ Mg_2SiO_4 + 4\ CaAl_2Si_2O_8 + 5\ SiO_2\ (aq) + 18\ H_2O = 2\ Ca_2Mg_5Si_8O_{22}(OH)_2 + 4\ Mg_5Al_2Si_3O_{10}(OH)_8$$

primary olivine   primary plagioclase   tremolite   chlorite   (3)

Although tremolite + chlorite could be produced by the removal of CaO or MgO from the reactants, the addition of SiO_2 is considered most effective because of the facts observed in Atlantis Massif gabbroic rocks: 1) association of coronitic tremolite and chlorite with talc replacing olivine; 2) uneven formation of the talc, in marked contrast to concentric tremolite-chlorite corona, suggestive of SiO_2 addition from infiltrated fluids; and 3) the formation of tremolite + chlorite + talc is significant in peridotite in direct contact with gabbroic rocks (Nozaka and Fryer 2011). The Hess Deep gabbroic rocks also contain talc with a similar mode of occurrence (Gillis et al. 2014b). Calculations using thermodynamic properties for minerals (Holland and Powell 1998) indicate that the volume proportion of chlorite/tremolite produced by Reaction 3 is ~1.5, which is consistent with petrographic observations, and that of total solid products/reactants is ~1.3. The volume expansion during this reaction possibly caused the microcracks filled with chlorite in plagioclase around the coronitic aggregates as suggested by Nozaka and Fryer (2011).

The reaction for the formation of tremolite + chlorite (Reaction 3) and those of spinel + pargasite (Reactions 1 and 2) indicate a gain and loss of SiO_2, respectively, suggesting a difference of chemical conditions. This difference is illustrated by the activity diagrams (Fig. 10) in which SiO_2 activities for spinel stability are much lower (< -0.3 log unit) than those for anorthite + chlorite stability or tremolite saturation at a given aMg^{2+}/a^2H^+ and aCa^{2+}/a^2H^+. These diagrams also indicate that a decrease of SiO_2 activity from a value for the primary assemblage of plagioclase + olivine is necessary for spinel formation but not for tremolite + chlorite formation. The difference in SiO_2 activity, and probably in acidity as well, between these mineral assemblages might reflect a discontinuity of hydrothermal activity.

Conditions of corundum and diaspore formation

Corundum and diaspore occur exclusively in contact with spinel in the studied samples. These two

minerals are undoubtedly the products of local alteration reactions around spinel grains, and indeed their stability fields do not appear in P-T pseudosections constructed from whole-rock compositions. Therefore, their formation conditions were examined in terms of phase diagrams for local equilibria between selected minerals in the simplified system $CaO-MgO-Al_2O_3-SiO_2-H_2O$. Corundum and chlorite could be produced by a reaction of spinel with aqueous fluids (Fig. 11a):

$$5\ MgAl_2O_4 + 3\ SiO_2\ (aq) + 4\ H_2O\quad =\quad 4\ Al_2O_3\quad +\quad Mg_5Al_2Si_3O_{10}(OH)_8\quad (4)$$

    spinel   corundum   chlorite

Diaspore pseudomorphs after corundum are in direct contact with chlorite surrounding spinel grains (Fig. 3b-g), which provides evidence that the reaction spinel = corundum + chlorite actually took place. The maximum temperature condition for this reaction was estimated to be 650-710 °C, assuming H_2O saturation, coexistence with spinel (X_{Mg} of 0.6-0.8) and the same pressure as the crystallization of spinel and amphibole + chlorite corona (Fig. 11b). However, the temperature could be lowered depending on SiO_2 activity (Fig. 11a). Considering the textural evidence for later formation of corundum from spinel, it is reasonable to infer a lower temperature for corundum than for the spinel formation. Figure 11 indicates that corundum + chlorite after spinel and tremolite + chlorite after olivine + plagioclase could be produced by fluids with similar SiO_2 activity under similar temperature conditions.

Diaspore is a hydration product of corundum at even lower temperatures (< 400 °C), probably similar to those attending serpentinization of olivine (Fig. 11).Tiny inclusions of iron sulfide in diaspore require the introduction of sulfur, and thus further invoke sulfate-bearing seawater. Harmonically, iron sulfides along with magnetite are commonly associated with serpentine replacing olivine as well. The physico-chemical conditions of the low-temperature alteration of the Hess Deep gabbros will be discussed elsewhere.

Concluding remarks

We observed and reported here for the first time aluminous spinel, corundum and diaspore in primitive troctolites recovered from *in-situ* oceanic crust at the Hess Deep Rift. They are the products of prolonged hydrothermal activity, and are significant because they monitor the history of interaction of seawater with lower crustal rocks. The formation conditions for spinel are the key to understanding the genesis of the

peculiar aluminous phases in the oceanic crust because corundum and diaspore need spinel as a reactant.

Textural observations, chemical analyses and thermodynamic modelling suggest that the spinel was produced along with pargasite and anorthite under a higher temperature (650-750 °C) than the widely reported amphibole-chlorite corona (410-690 °C). The stabilization of spinel was caused by the loss of Ca and SiO_2, which resulted from local metasomatic reactions around magmatic plagioclase and removal by high-temperature hydrothermal fluids. In fact, the spinel + pargasite assemblage could be produced, without extraordinary geologic conditions and processes, by the incompatibility of anorthite + olivine, which is the typical assemblage of primitive troctolites. Therefore, metamorphic spinel and postdating corundum and diaspore could be widely present, or chemical modification due to high-temperature hydrothermal activities could widely take place in the lower oceanic crust near spreading axes.

Acknowledgments

References

Abily B, Ceuleneer G, Launeau P (2011) Synmagmatic normal faulting in the lower oceanic crust: Evidence from the Oman ophiolite. Geology 39:391-394

Bach W, Klein F (2009) The petrology of seafloor rodingites: Insights from geochemical reaction path

modeling. Lithos 112:103-117

Bach W, Garrido CJ, Paulick H, Harvey J, Rosner M (2004) Seawater-peridotite interactions: First insights from ODP Leg 209, MAR 15°N. Geochem Geophys Geosyst doi:10.1029/2004GC000744

Bence AE, Albee AL (1968) Empirical correction factors for the electron microanalysis of silicates and oxides. J Geol 76:382-403

Connolly JAD (2005) Computation of phase equilibria by linear programming: A tool for geodynamic modeling and its application to subduction zone decarbonation. Earth Planet Sci Lett 236:524-541

Connolly JAD (2009) The geodynamic equation of state: What and how. Geochem Geophys Geosyst doi:10.1029/2009GC002540

Coogan LA, Gillis KM, MacLeod CJ., Thompson G M, Hékinian R (2002) Petrology and geochemistry of the lower ocean crust formed at the East Pacific Rise and exposed at Hess Deep: A synthesis and new results. Geochem Geophys Geosyst doi:10.1029/2001GC000230

Deer W A, Howie R A, Zussman J (1992) An introduction to the rock-forming minerals. John Wiley and Sons, New York

Dick HJB, Tivey MA, Tucholke BE (2008) Plutonic foundation of a slow-spreading ridge segment: Oceanic core complex at Kane Megamullion, 23°30'N, 45°20'W. Geochem Geophys Geosyst doi:10.1029/2007GC001645

Diener JFA, Powell R, White RW, Holland TJB (2007) A new thermodynamic model for clino- and orthoamphiboles in the system Na_2O-CaO-FeO-MgO-Al_2O_3-SiO_2-H_2O-O. J Metamorph Geol 25:631-656

Dolejš D, Manning CE (2010) Thermodynamic model for mineral solubility in aqueous fluids: theory, calibration and application to model fluid-flow systems. Geofluids 10:20-40

Ferry JM (1985) Hydrothermal alteration of Tertiary igneous rocks from the Isle of Skye, northwest Scotland. I. Gabbros. Contrib Mineral Petrol 91:264-282

Francheteau J, Armijo R, Cheminée JL, Hékinian R, Lonsdale P, Blum N (1990) 1 Ma East Pacific Rise oceanic crust and uppermost mantle exposed by rifting in Hess Deep (equatorial Pacific Ocean). Earth Planet Sci Lett 101:281-295

Gillis KM, Snow JE, Klaus A, Abe N, Adrião AB, Akizawa N, Ceuleneer G, Cheadle MJ, Faak K, Falloon TJ, Friedman SA, Godard M, Guerin G, Harigane Y, Horst AJ, Hoshide T, Ildefonse B, Jean

MM, John BE, Koepke J, Machi M, Maeda J, Marks NE, McCaig AM, Meyer R, Morris A, Nozaka T, Python M, Saha A, Wintsch RP (2014a) Primitive layered gabbros from fast-spreading lower oceanic crust. Nature 505:204-207

Gillis KM, Snow JE, Klaus A, the Expedition 345 Scientists (2014b) Hess Deep Plutonic Crust: Exploring the Plutonic Crust at a Fast-Spreading Ridge: New Drilling at Hess Deep. Proc IODP 345 doi:10.2204/iodp.proc.345.2014

Hékinian R, Bideau D, Francheteau J, Cheminee J, Armijo R, Lonsdale P, Blum N (1993) Petrology of the East Pacific Rise crust and upper mantle exposed in Hess Deep (eastern Equatorial Pacific). J Geophys Res 98:8069-8094

Holland TJB, Powell R (1991) A Compensated-Redlich-Kwong (CORK) equation for volumes and fugacities of CO_2 and H_2O in the range 1 bar to 50 kbar and 100–1600°C. Contrib Mineral Petrol 109:265-273

Holland T, Powell R (1996) Thermodynamics of order-disorder in minerals. II. Symmetric formalism applied to solid solutions. Am Mineral 81:1425-1437

Holland TJB, Powell R (1998) An internally consistent thermodynamic data set for phases of petrological interest. J Metamorph Geol 16:309-343

Holland T, Powell R (2003) Activity-composition relations for phases in petrological calculations: an asymmetric multicomponent formulation. Contrib Mineral Petrol 145:492-501

Holland TJB, Powell R (2011) An improved and extended internally consistent thermodynamic dataset for phases of petrological interest, involving a new equation of state for solids. J Metamorph Geol 29:333-383

Holland T, Baker J, Powell R (1998) Mixing properties and activity-composition relationships of chlorites in the system MgO-FeO-Al_2O_3-SiO_2-H_2O. Eur J Mineral 10:395-406

Johnson JW, Oelkers EH, Helgeson HC (1992) SUPCRT92: a software package for calculating the standard molal thermodynamic properties of minerals, gases, aqueous species, and reactions from 1 to 5000 bar and 0 to 1000 °C. Comput Geosci 18:899–947.

Kirchner TM, Gillis KM (2012) Mineralogical and strontium isotopic record of hydrothermal processes in the lower ocean crust at and near the East Pacific Rise. Contrib Mineral Petrol 164:123-141

Kornprobst J, Piboule M, Roden M, Tabit A (1990) Corundum-bearing garnet clinopyroxenites at Beni

Bousera (Morocco): Original plagioclase-rich gabbros recrystallized at depth within the mantle? J Petrol 31:717-745

Lissenberg CJ, MacLeod CJ, Howard KA, Godard M (2013) Pervasive reactive melt migration through fast-spreading lower oceanic crust (Hess Deep, equatorial Pacific Ocean). Earth Planet Sci Lett 361:436-447

Lonsdale P (1988) Structural pattern of the Galapagos microplate and evolution of the Galapagos triple junctions. J Geophys Res 93:13551-13574

Maclennan J, Hulme T, Singh SC (2004) Thermal models of oceanic crustal accretion: Linking geophysical, geological and petrological observations. Geochem Geophys Geosyst doi:10.1029/2003GC000605

Manning CE, MacLeod CJ (1996) Fracture-controlled metamorphism of Hess Deep gabbros, Site 894: constraints on the roots of mid-ocean-ridge hydrothermal systems at fast-spreading centers. Proc ODP Sci Res 147:189-212

Manning CE, Weston PE, Mahon KI (1996) Rapid high-temperature metamorphism of East Pacific Rise gabbros from Hess Deep. Earth Planet Sci Lett 144:123-132

Mével C, Gillis KM, Shipboard Scientific Party (1993) Introduction and principal results. Proc ODP Init Repts 147:5-14

Morishita T, Arai S (2001) Petrogenesis of corundum-bearing mafic rock in the Horoman peridotite complex, Japan. J Petrol 42:1279-1299

Nakamura Y, Kushiro I (1970) Compositional relations of coexisting orthopyroxene, pigeonite and augite in a tholeiitic andesite from Hakone volcano. Contrib Mineral Petrol 26:265-275

Nozaka T, Fryer P (2011) Alteration of the oceanic lower crust at a slow-spreading axis: Insight from vein-related zoned halos in olivine gabbro from Atlantis Massif, Mid-Atlantic Ridge. J Petrol 52: 643-664

Rioux M, Lissenberg CJ, McLean NM, Bowring SA, MacLeod CJ, Hellebrand E, Shimizu N (2012) Protracted timescales of lower crustal growth at the fast-spreading East Pacific Rise. Nature Geosci 5:275-278

Rouméjon S, Cannat M, Agrinier P, Godard M, Andreani M (2015) Serpentinization and fluid pathways in tectonically exhumed peridotites from the Southwest Indian Ridge (62-65°E). J Petrol 56:703-734

16

Sauter D, Cannat M, Rouméjon S, Andreani M, Birot D, Bronner A, Brunelli D, Carlut J, Delacour A, Guyader V, MacLeod CJ, Manatschal G, Mendel V, Ménez B, Pasini V, Ruellan E, Searle R (2013) Continuous exhumation of mantle-derived rocks at the Southwest Indian Ridge for 11 million years. Nature Geosci 6:314-320

Seyfried WE Jr (1987) Experimental and theoretical constraints on hydrothermal alteration processes at mid-ocean ridges. Ann Rev Earth Planet Sci 15:317-335

Shock EL, Helgeson HC, Sverjensky DA (1989) Calculations of the thermodynamic and transport properties of aqueous species at high pressures and temperatures: standard partial molal properties of inorganic neutral species. Geochim Cosmochim Acta 53:2157–2183

Stefánsson A (2001) Dissolution of primary minerals of basalt in natural waters: I. Calculation of mineral solubilities from 0°C to 350°C. Chem Geol 172:225-250

Wiggins SM, Dorman LM, Cornuelle BD, Hildebrand JA (1996) Hess Deep rift valley structure from seismic tomography. J Geophys Res 101:22335-22353

Zimmer K, Zhang Y, Lu P, Chen Y, Zhang G, Dalkilic M, Zhu C (2016) SUPCRTBL: A revised and extended thermodynamic dataset and software package of SUPCRT92. Comp Geosci 90:97-111

Zonenshain LP, Kogan LI, Savostin LA, Golmstock AJ, Gorodnitskii AM (1980) Tectonics, crustal structure and evolution of the Galapagos triple junction. Mar Geol 37:209-230

Table 1 Representative microprobe analyses of minerals

Sample	U1415J-18R-1_8-14 cm										U1415J-13R-1_59-64 cm					
Mineral	Ol (P)	Pl (P)	Sp (P)	Parg	Tr	Pl	Chl	Sp	Co	Dsp	Ol (P)	Cpx (P)	Pl (P)	Sp (P)	Tr	Chl
SiO$_2$	40.18	45.53	0.08	45.11	58.09	42.75	27.48	0.01	<0.01	<0.01	39.73	39.75	46.69	<0.01	57.76	31.55
TiO$_2$	n.d.	0.04	1.72	0.06	0.02	0.02	0.04	<0.02	0.02	<0.02	n.d.	<0.02	<0.02	1.49	0.03	<0.02
Al$_2$O$_3$	n.d.	33.70	11.48	13.10	0.09	36.16	23.05	66.55	98.14	80.84	n.d.	<0.02	33.98	17.21	0.02	17.56
Cr$_2$O$_3$	n.d.	n.d.	42.21	<0.02	<0.02	n.d.	<0.02	0.07	0.03	0.02	n.d.	0.02	n.d.	43.06	<0.02	<0.02
FeO*	11.93	8.86	38.56	5.82	1.58	0.06	8.20	9.80	0.31	0.38	11.74	11.42	0.33	26.54	1.35	4.15
MnO	0.20	<0.02	1.43	0.10	0.04	<0.02	0.05	0.05	0.02	<0.02	0.17	0.22	<0.02	0.52	0.10	0.07
NiO	0.26	n.d.	0.21	0.13	0.19	n.d.	0.13	0.26	<0.04	<0.04	0.25	0.26	n.d.	0.05	0.12	0.16
MgO	47.15	0.14	3.07	17.57	23.22	0.01	25.71	21.65	<0.01	0.03	47.73	48.08	0.09	10.88	23.92	31.28
CaO	0.05	18.18	0.06	12.79	13.90	20.31	0.03	0.01	<0.01	0.01	0.06	0.05	18.15	0.03	13.88	0.03
Na$_2$O	n.d.	1.36	n.d.	2.02	0.03	0.16	0.01	n.d.	<0.01	<0.01	n.d.	<0.01	1.50	n.d.	0.01	0.01
K$_2$O	n.d.	<0.01	n.d.	0.08	0.01	<0.01	0.01	n.d.	<0.01	<0.01	n.d.	0.01	0.03	n.d.	0.01	0.01
Total	99.78	99.35	98.82	96.78	97.17	99.46	84.71	98.40	98.51	81.29	99.68	99.82	100.80	99.78	97.18	84.81
O	4	8	4	23	23	8	14	4	3	3	4	6	6	4	23	14
Si	1.00	2.12	<0.01	6.47	7.98	1.99	2.72	<0.01	<0.01	<0.01	0.99	1.48	2.14	<0.01	7.93	3.06
Ti	n.d.	<0.01	0.05	0.01	<0.01	<0.01	<0.01	<0.01	<0.01	<0.01	n.d.	<0.01	<0.01	0.04	<0.01	<0.01
Al	n.d.	1.85	0.49	2.21	0.01	1.99	2.69	1.98	2.00	1.99	n.d.	<0.01	1.83	0.66	<0.01	2.01
Cr	n.d.	n.d.	1.20	<0.01	<0.01	n.d.	<0.01	<0.01	<0.01	<0.01	n.d.	<0.01	n.d.	1.11	<0.01	<0.01
Fe	0.25	0.18	1.16	0.70	0.18	<0.01	0.68	0.21	<0.01	0.01	0.24	0.36	0.01	0.72	0.16	0.34
Mn	<0.01	<0.01	0.04	0.01	0.01	<0.01	<0.01	<0.01	<0.01	<0.01	<0.01	0.01	<0.01	0.01	0.01	<0.01
Ni	0.01	n.d.	0.01	0.01	0.02	n.d.	0.01	0.01	<0.01	<0.01	0.01	0.01	n.d.	<0.01	0.01	0.01
Mg	1.75	0.01	0.16	3.76	4.76	<0.01	3.80	0.81	<0.01	<0.01	1.77	2.67	0.01	0.53	4.90	4.52
Ca	<0.01	0.91	<0.01	1.96	2.05	1.02	<0.01	<0.01	<0.01	<0.01	<0.01	<0.01	0.89	<0.01	2.04	<0.01
Na	n.d.	0.12	n.d.	0.56	0.01	0.01	<0.01	n.d.	<0.01	<0.01	n.d.	<0.01	0.13	n.d.	<0.01	<0.01
K	n.d.	<0.01	n.d.	0.01	<0.01	<0.01	<0.01	n.d.	<0.01	<0.01	n.d.	<0.01	<0.01	n.d.	<0.01	<0.01
Total	3.00	5.02	3.11	15.71	15.01	5.02	9.93	3.01	2.00	2.00	3.01	4.52	5.01	3.08	15.06	9.94
X$_{Mg}$	0.876	-	0.124	0.843	0.963		0.848	0.797	-	-	0.878	0.882		0.422	0.969	0.931
An	-	88.1	-	-	-	98.6	-	-	-	-	-	-	87.0	-	-	-

* Total iron as FeO. n.d., not determined; X$_{Mg}$ = Mg/(Mg+Fe); An = 100Ca/(Ca+Na). Abbreviations: Chl, chlorite; Co, corundum; Cpx, clinopyroxene; Dsp, diaspore; Ol, olivine; Parg, pargasite; Pl, plagioclase; Sp, spinel; Tr, tremolite; (P), primary phase.

Table 2 Major-element compositions of altered troctolites from IODP U1415 Hole J

Sample	13R1_59-64 cm	18R1_8-14 cm	18R1_59-62 cm	18R1_62-65 cm	18R1_67-69 cm	19R1_39-45 cm
Modal spinel	absent	present	present	present	present	absent
SiO$_2$ (wt%)	44.88	42.76	42.43	41.49	39.36	42.90
TiO$_2$	0.05	0.04	0.03	0.03	0.05	0.06
Al$_2$O$_3$	13.39	18.56	13.39	14.70	12.34	8.41
FeO*	7.09	5.69	7.25	9.03	16.68	8.08
MnO	0.11	0.06	0.04	0.05	0.05	0.13
MgO	25.23	22.58	28.60	26.96	21.47	32.96
CaO	7.37	8.41	6.24	5.98	7.01	6.00
Na$_2$O	0.46	0.38	0.42	0.23	0.48	0.16
K$_2$O	0.10	0.07	0.04	0.03	0.10	0.05
P$_2$O$_5$	0.01	0.00	0.01	0.01	0.01	0.01
Total	98.69	98.55	98.45	98.51	97.55	98.76
LOI	7.41	6.44	7.53	7.89	5.62	9.15
Mg#	86.4	87.6	87.5	84.2	69.6	87.9
CIPW norm						
Quartz (wt%)	-	-	-	-	-	-
Corundum	-	2.57	1.31	3.42	-	-
Nepheline	-	-	-	-	1.67	-
Feldspar	38.66	45.34	34.74	31.78	32.80	23.73
Diopside	1.89	-	-	-	2.88	6.08
Hypersthene	15.73	10.64	7.40	11.81	-	6.24
Olivine	42.32	39.92	54.94	51.43	60.10	62.59
Ilmenite	0.09	0.08	0.06	0.06	0.09	0.11

* Total iron as FeO. LOI = loss on ignition.
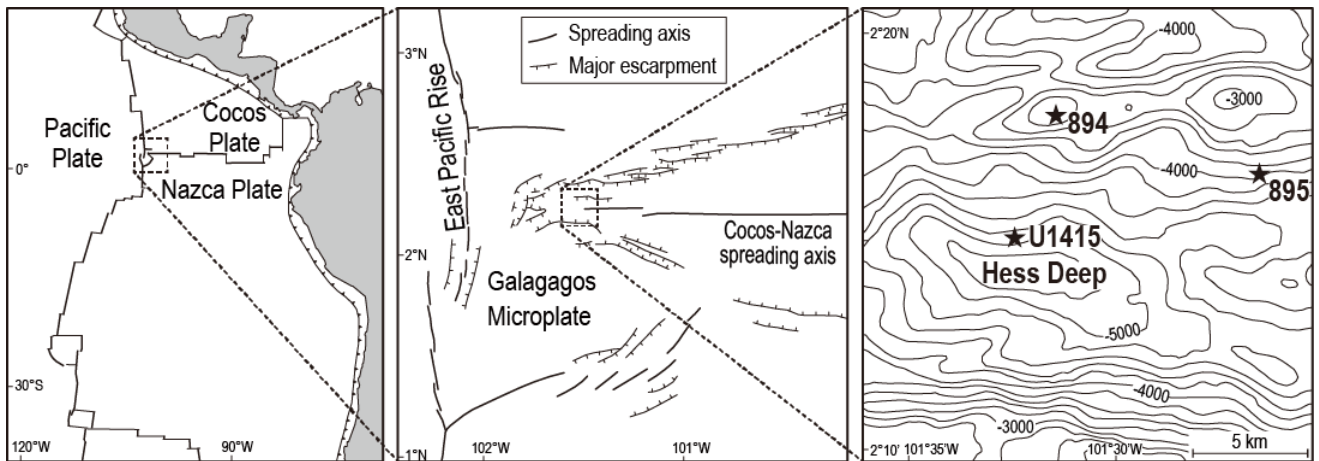
Fig. 1 Locality and bathymetric maps of the Hess Deep Rift area showing the drilling sites: IODP Site U1415, ODP Site 894 and ODP Site 895 (Lonsdale 1988; Mével et al. 1993; Gillis et al. 2014b)
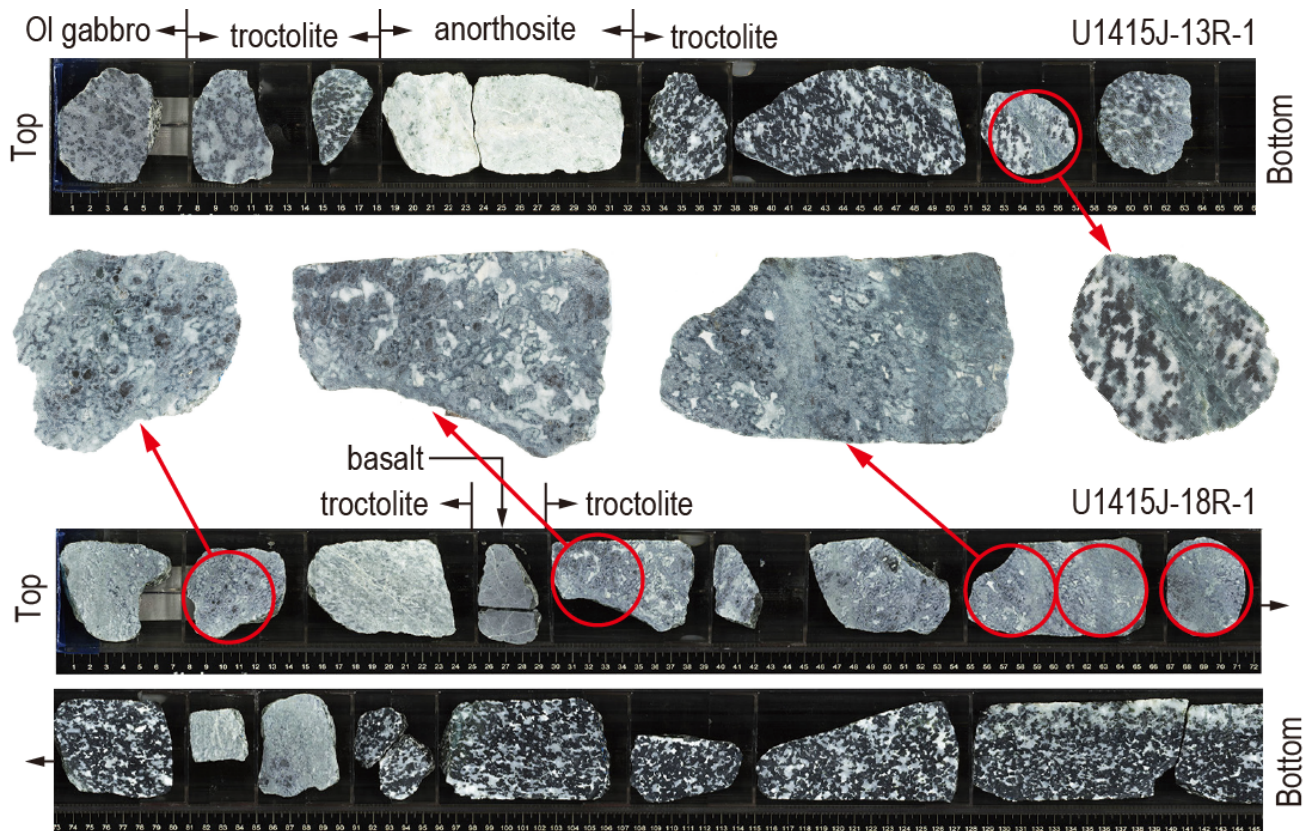
Fig. 2 Photographs of split cores with petrographically observed green spinel (Section U1415J-13R-1 and U1415J-18R-1). Circles indicate green spinel locations examined in this study
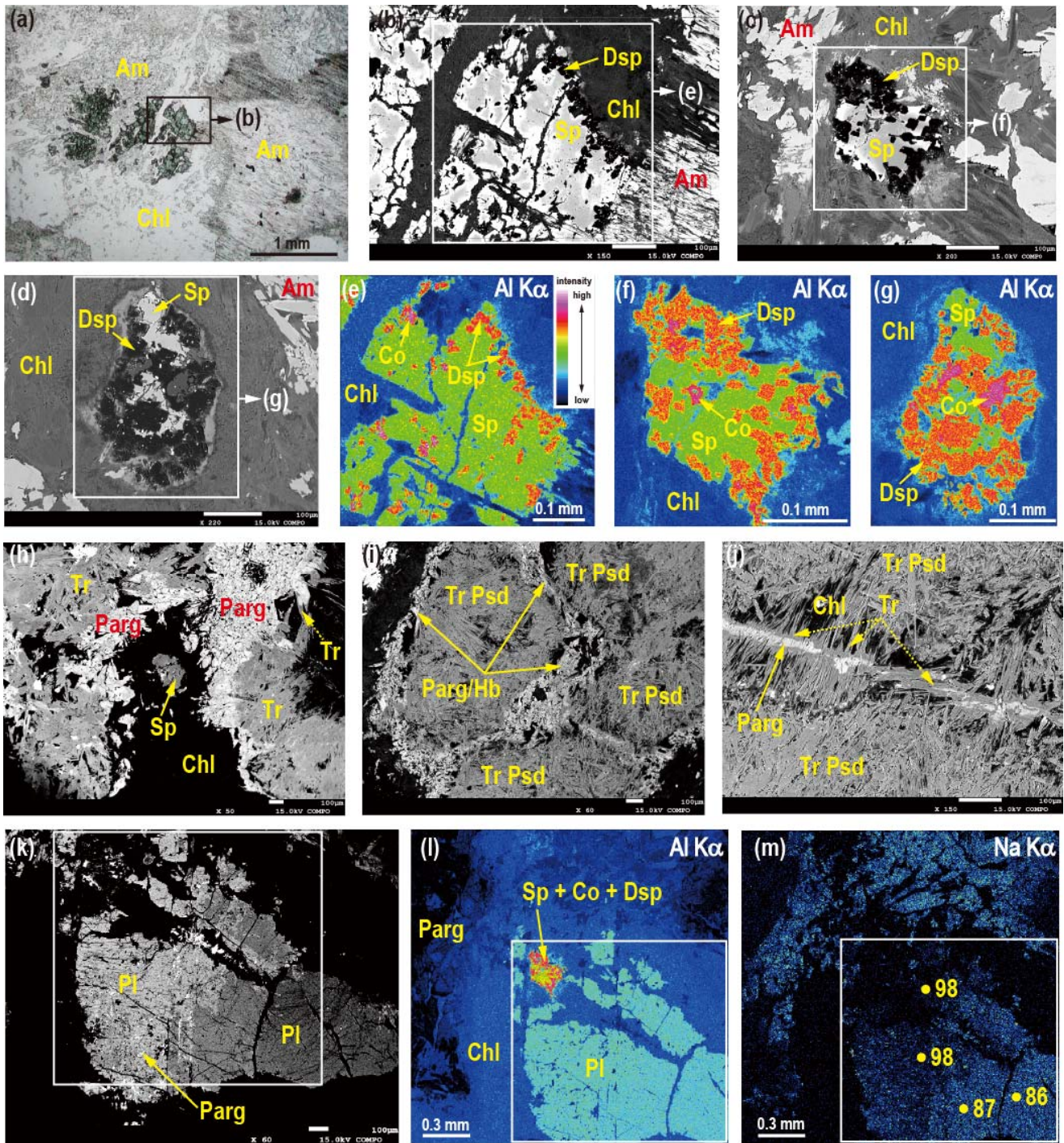
Fig. 3 Modes of occurrence of green spinel and associated minerals. **a** Photomicrograph (PPL) of anhedral spinel grains in sample U1415J-18R-1_59-62 cm. **b** Back-scattered electron image of a part of **a**. Tiny bright spots within diaspore are iron sulfide grains. **c, d** Back-scattered electron image around a spinel grain in sample U1415J-18R-1_8-14 cm. **e** Al-Kα X-ray map of a part of **a** and **b**. Corundum shows a slightly higher Al-Kα intensity than diaspore. **f** Al-Kα X-ray map of a part of **c**. **g** Al-Kα X-ray

map of a part of **d**. **h** Back-scattered electron image showing a compositional variation of amphibole surrounding a spinel grain in sample U1415J-18R-1_8-14 cm. Dotted arrow indicates tremolite overgrowth on pargasite. **i, j** Back-scattered electron image showing a compositional variation of amphibole forming pseudomorphic aggregates after olivine in sample U1415J-18R-1_62-65 cm. Tremolite overgrows on pargasite (dotted arrow). **k** Back-scattered electron image showing a compositional variation of plagioclase near a spinel grain in sample U1415J-18R-1_8-14 cm. Bright spots in plagioclase are pargasite inclusions. Square is the same area as those of **l** and **m**. **l** Al-Kα X-ray map around the area of **k**. **m** Na-Kα X-ray map of the same area as **l**. Dots are the points of quantitative analysis and numbers indicate anorthite (An) contents (mol%) of plagioclase. The plagioclase with An content of 86-87 and without pargasite inclusion is an unaltered part of primary grain of igneous origin. Abbreviations: Am, amphibole; Chl, chlorite; Co, corundum; Dsp, diaspore; Hb, hornblende; Parg, pargasite; Pl plagioclase; Sp, spinel; Tr, tremolite; Tr Psd, pseudomorphic aggregate of tremolite after olivine
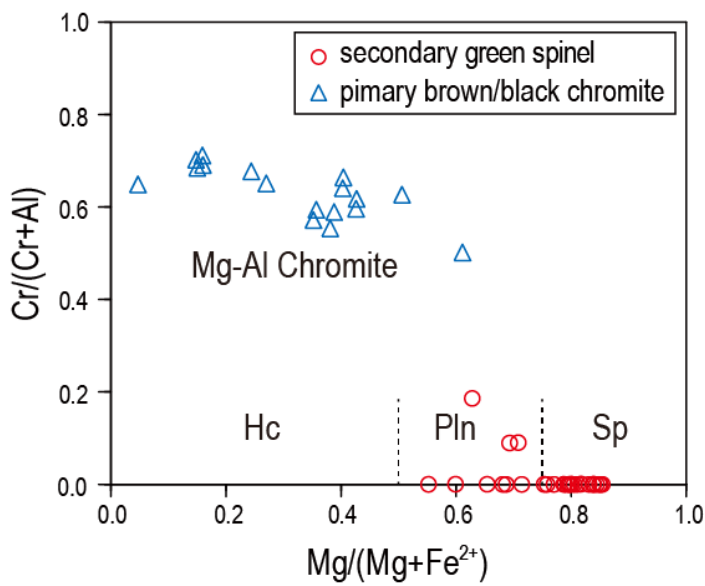
Fig. 4 Cr/(Cr+Al) vs Mg/(Mg+Fe^{2+}) ratios of spinel. Fe^{2+} and Fe^{3+} were calculated from total iron on the basis of spinel stoichiometry. Classification of spinel follows Deer et al. (1992). Abbreviations: Hc, hercynite; Pln, pleonaste; Sp, spinel
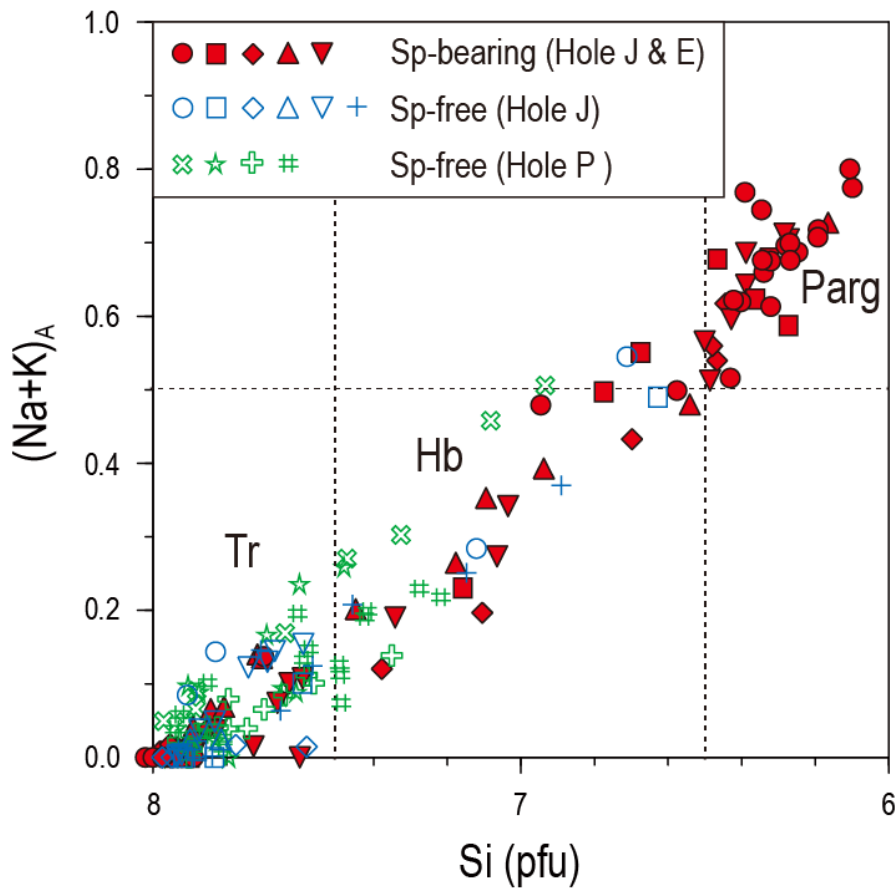
24

Fig. 5 Na+K (in A site) vs Si per formula unit (pfu) of amphibole. Na (A site) was calculated assuming Ca+Na (B sites) = 2, total iron = Fe^{2+} and O = 23. Classification of amphibole follows Deer et al. (1992). Each symbol is used for amphiboles from the same thin section of spinel-bearing (solid symbols) and spinel-free samples (open symbols and crosses). Abbreviations: Hb, hornblende; Parg, pargasite; Sp, spinel; Tr, tremolite
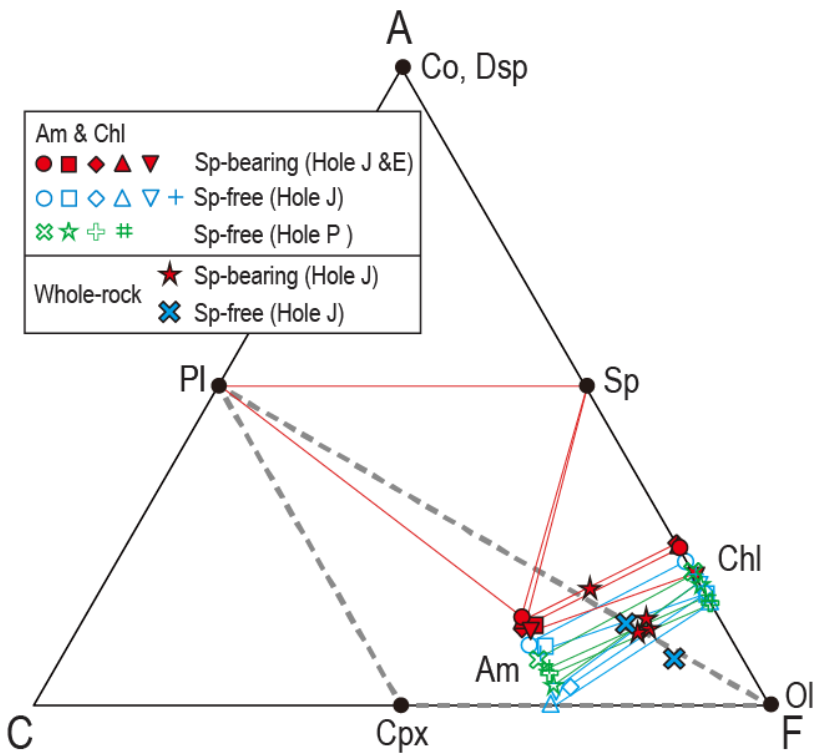
Fig. 6 ACF (molar Al_2O_3 - Na_2O - K_2O, CaO and FeO + MgO + MnO) diagram showing relationships between assemblages and chemical compositions of minerals. Total iron is assumed to be FeO. Amphibole and chlorite with the maximum Al_2O_3 content in each sample are plotted, and representative assemblages are connected with solid tie-lines. Dashed tie-lines indicate the primary assemblage. Symbols for amphibole and coexisting chlorite are the same as those of Fig. 5. Whole-rock compositions (Table 2) are also plotted. Abbreviations: Am, amphibole; Chl, chlorite; Co, corundum; Cpx, clinopyroxene; Dsp, diaspore; Ol, olivine; Pl, plagioclase; Sp, spinel
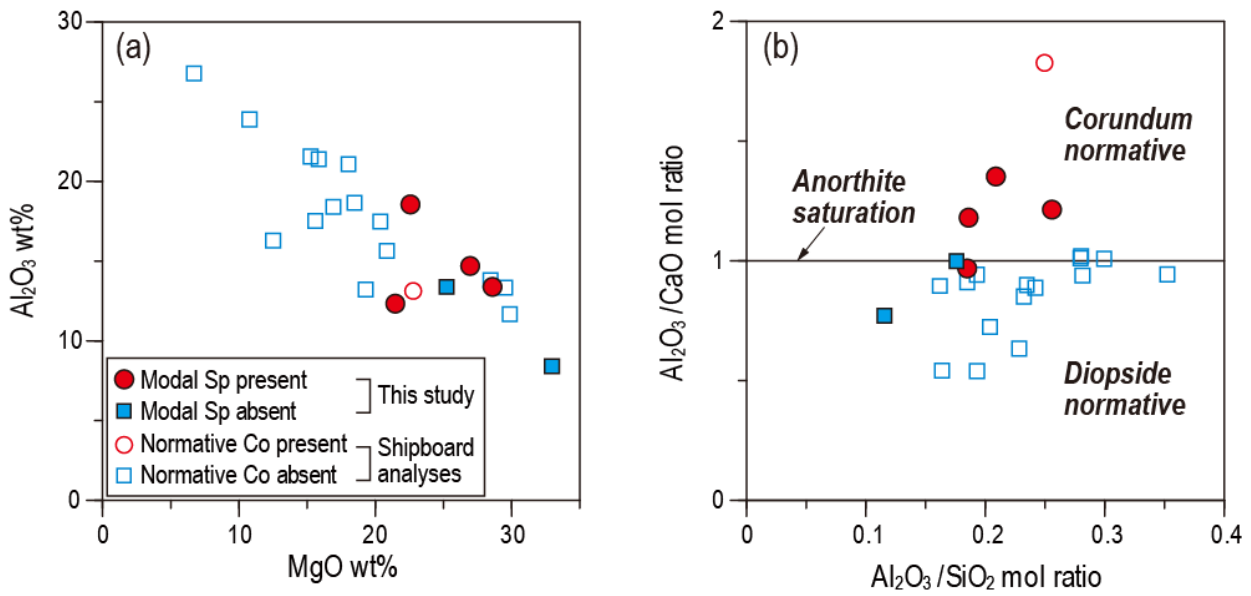
Fig. 7 Variations of rock composition and their relation with the existence of modal spinel or normative corundum. Shipboard analyses of troctolites and gabbros (Gillis et al. 2014b) are also plotted. **a** Al_2O_3 wt% vs MgO wt%; **b** Al_2O_3/CaO vs Al_2O_3/SiO_2 mol ratios
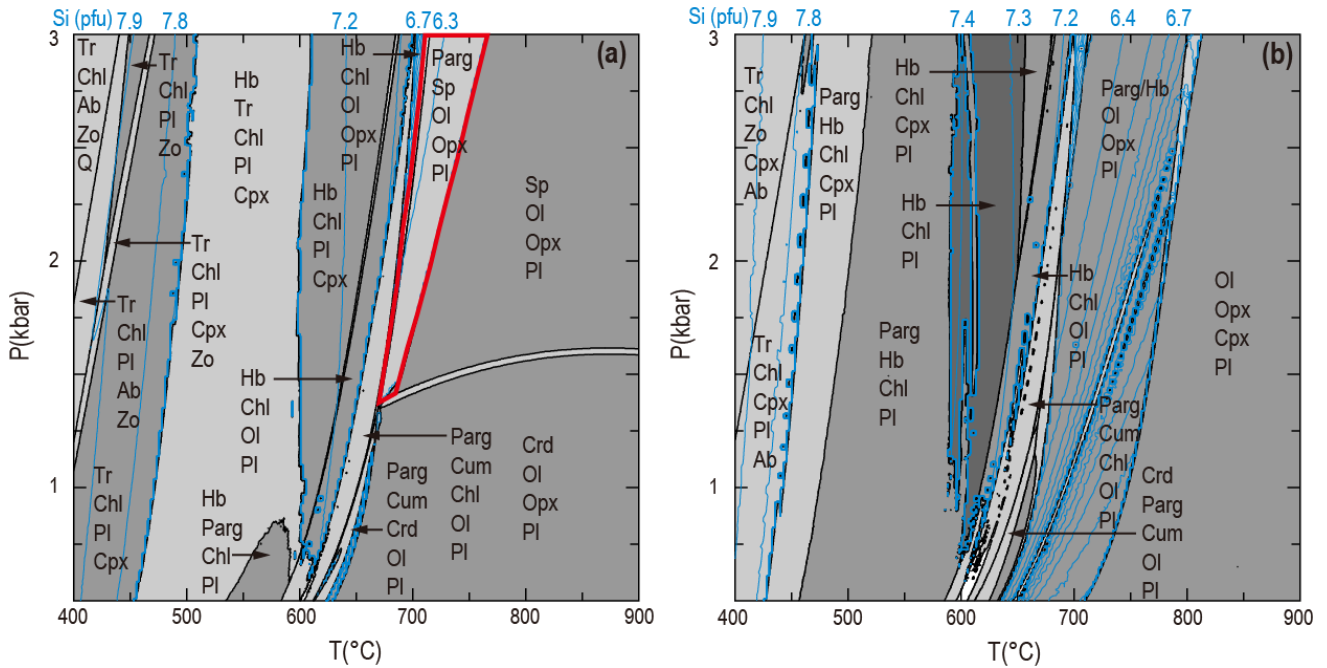
Fig. 8 Representative P-T pseudosections in the system Na_2O-CaO-FeO-MgO-Al_2O_3-SiO_2-H_2O with H_2O saturation constructed using the software Perple_X ver. 6.6.8 with the dataset of Holland and Powell (1998, updated 2002) for **a** spinel-bearing sample (U1415J-18R-1_8-14 cm); **b** spinel-free sample (U1415J-13R-1_59-64 cm). Isopleths of Si contents (pfu) of calcic amphibole are also shown (thin lines). The stability field of spinel + pargasite is enclosed by thick lines. Abbreviations: Ab, albite; Chl, chlorite; Cpx, clinopyroxene; Crd, cordierite; Cum, cummingtonite; Hb, hornblende; Ol, olivine; Opx, orthopyroxene; Parg, pargasite; Pl plagioclase; Q, quartz; Sp, spinel; Tr, tremolite; Zo, zoisite
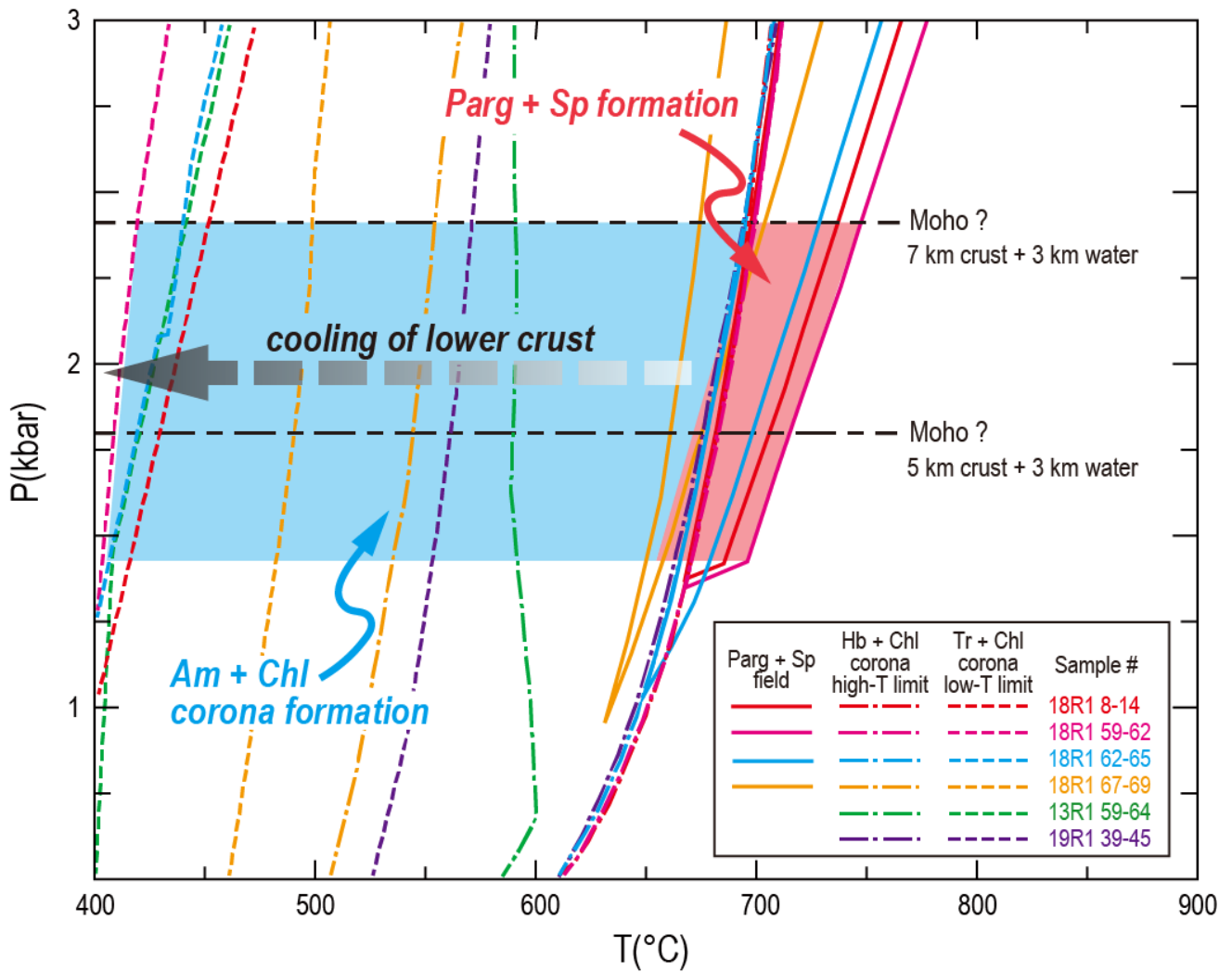
Fig. 9 P-T conditions for spinel and corona formation estimated from the integration of P-T pseudosections of six samples (Table 2) drawn using the software Perple_X ver. 6.6.8 with the dataset of Holland and Powell (1998, updated 2002). Likely conditions for pargasite + spinel formation at Hess Deep are inferred from the overlap of the stability fields of all samples and seismic Moho depth (Zonenshain et al. 1980). Abbreviations are given in Figs. 6 and 8
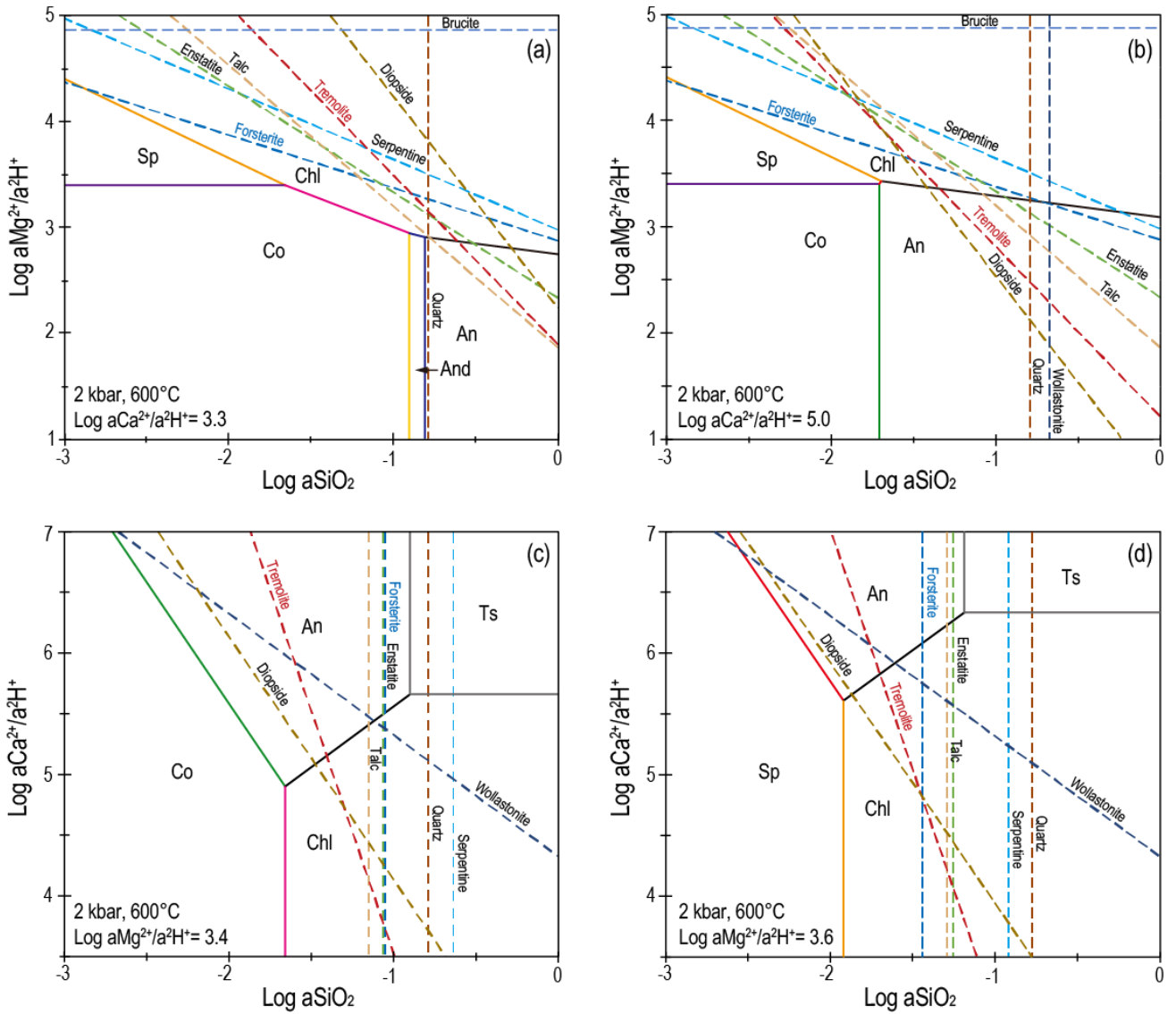
Fig. 10 Aqueous activity diagrams of the system CaO-MgO-Al$_2$O$_3$-SiO$_2$-H$_2$O at 2.0 kbar, 600 °C and H$_2$O saturation constructed using the software SUPCRT (see methods) and following the computation methods of Zimmer et al. (2016). **a** aMg^{2+}/a^{2}H$^+$ vs aSiO$_2$ (aq) at log aCa^{2+}/a^{2}H$^+$ = 3.3; **b** aMg^{2+}/a^{2}H$^+$ vs aSiO$_2$ (aq) at log aCa^{2+}/a^{2}H$^+$ = 5.0; **c** aCa^{2+}/a^{2}H$^+$ vs aSiO$_2$ (aq) at log aMg^{2+}/a^{2}H$^+$ = 3.4; and **d** aCa^{2+}/a^{2}H$^+$ vs aSiO$_2$ (aq) at log aMg^{2+}/a^{2}H$^+$ = 3.6. The stability fields of aluminous phases and saturation curves of related minerals are shown by solid and dashed lines, respectively. Abbreviations: An, anorthite; And, andalusite; Chl, clinochlore; Co, corundum; Sp, spinel; Ts, tschermakite
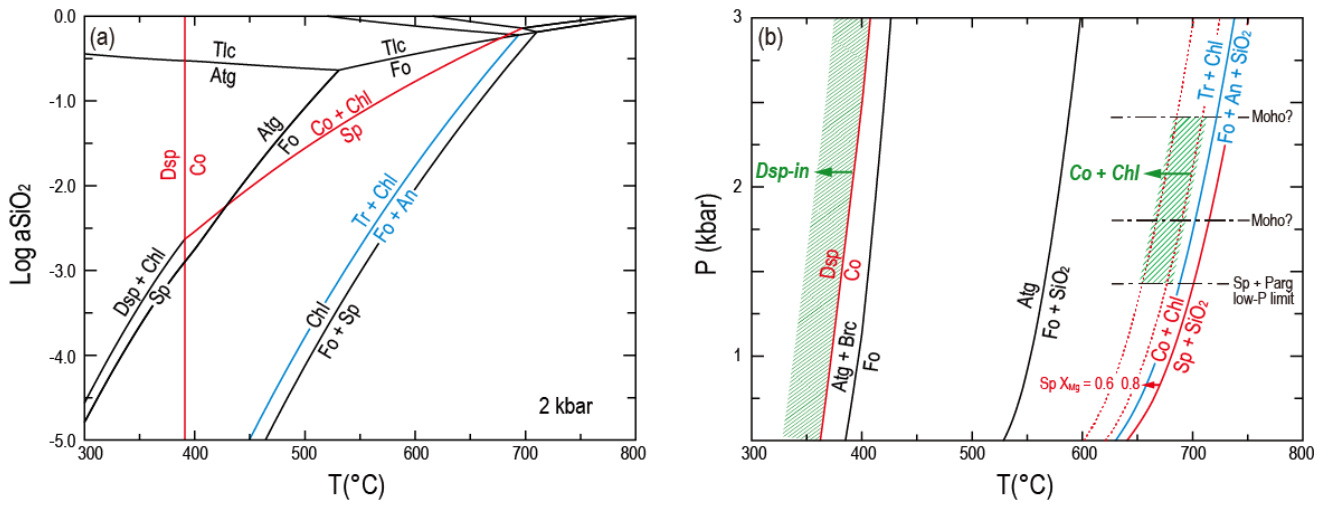
Fig. 11 Phase diagrams showing physico-chemical conditions for the formation of corundum and diaspore in the system CaO-MgO-Al$_2$O$_3$-SiO$_2$-H$_2$O with H$_2$O saturation constructed using the software Perple_X ver. 6.6.8 with the dataset of Holland and Powell (1998, updated 2002). **a** SiO$_2$ (quartz) activity vs temperature diagram at 2 kbar; **b** P-T diagram. Dotted lines indicate the effect of substitution of Fe for Mg in spinel. Pressure limits for corundum formation are inferred from those for spinel + pargasite (Fig. 9). Abbreviations: An, anorthite; Atg, antigorite; Brc, brucite; Chl, clinochlore; Co, corundum; Dsp, diaspore; Fo, forsterite; Sp, spinel; Tlc, talc; Tr, tremolite